



High-order harmonics generation in Cd and Pd laser-induced plasmas

RASHID A. GANEEV,^{1,2,3,4,*}  VYACHESLAV V. KIM,^{1,2} JELENA BUTIKOVA,⁵ AIGARS ATVARIS,¹  JURGIS GRUBE,⁵  ANATOLIJS SARAKOVSKIS,⁵ AND ARNOLDS UBELIS⁶

¹Laboratory of Nonlinear Optics, University of Latvia, Jelgavas 3, Riga, LV – 1004, Latvia

²Institute of Fundamental and Applied Research, TIAME National Research University, Kori Niyoziy 39, Tashkent 100000, Uzbekistan

³Chirchik State Pedagogical University, 104 Amir Temur, Chirchik 111700, Uzbekistan

⁴Department of Physics, Voronezh State University, Voronezh 394006, Russia

⁵Institute of Solid State Physics, University of Latvia, Kengaraga 8, Riga, LV-1063, Latvia

⁶National Science Platform FOTONIKA-LV, University of Latvia, Šķūņu iela 4, Riga, LV-1050, Latvia

*rashid.ganeev@lu.lv

Abstract: We demonstrate the generation of high-order harmonics of laser pulses in palladium and cadmium plasmas. We adjusted the wavelength of driving pulses to investigate the resonance enhancement in different ranges of extreme ultraviolet region. The summation of incommensurate waves during the two-color pump of Pd and Cd plasmas allowed the generation of a broader range of harmonics. The theoretical aspects of the two-color pump of the laser-induced plasma are discussed.

© 2023 Optica Publishing Group under the terms of the [Optica Open Access Publishing Agreement](#)

1. Introduction

High-order harmonics generation (HHG) is a well-recognized and relevant method to produce coherent extreme ultraviolet (XUV) radiation sources. In general, the broad pattern in the developments of HHG includes the application of this process in gases [1–5], solids [6,7], plasmas [8–10], and during specular reflection from the surfaces [11–13]. One of those methods, HHG in laser-induced plasmas, is an advanced approach for creating coherent radiation sources in the XUV region for different purposes. It can be used for the studies of materials through the analysis of their properties by applying the unique method of nonlinear spectroscopy related to HHG of ultrashort laser pulses in laser-ablated samples. The development of new approaches in the determination of the atomic and optical characteristics of materials through the application of advanced methods allows the growth of high-order harmonic yield using clusters, quantum dots, nanoparticles, extended plasmas, two- and three-color pumps, resonance enhancement of single harmonic in the vicinity of strong ionic transitions, application of quasi-phase-matching conditions, etc. are the potential goals of laser-ablation induced HHG spectroscopy [14–43].

Among the potential fundamental results of the development of HHG in ablated materials are diagnostics of laser-induced and other plasmas, the search for improvement and understanding of the fine structure of the energy levels of atoms and ions, etc. The practical aspects of this approach include the formation of an intense coherent radiation source in the XUV spectral range. Other aspects related to the practical use of plasma harmonics may include such competitive fields as biomedicine, biology, microscopy, research on the properties of materials, etc.

The formation of the sources of coherent XUV sources requires the determination of the efficient plasma media allowing large harmonic yield HHG [44–50]. An analysis of the metal elements belonging to the fifth period of the periodic table as the targets for optimal laser-induced plasma (LIP) formation resulted in the determination of some of them (Mo, Ag, In, Sn, and Sb) demonstrating the best conditions for harmonics generation. Two other metals of the fifth period

of a table (Pd and Cd) can also be treated as the perspective plasma media for HHG at the optimal conditions of plasma formation, particularly by using laser-induced breakdown spectroscopy (LIBS). Notice that laser-induced silver (atomic number 47, the metal between Pd and Cd in the table) plasma during a single-color pump (SCP), as well as a two-color pump (TCP), of LIP proved to be the most efficient media among all metals for HHG [51].

Previously, TCP of LIPs used commensurate waves (i.e., waves representing some integers with regard to each other). Meanwhile, the application of incommensurate waves for TCP of gases and plasmas showed the advantages in harmonic yield [52,53] and shortening of harmonic pulse duration thus allowing the generation of attosecond pulses using the multicycle laser sources [54].

In this paper, we describe the studies of plasma formation using LIBS during laser ablation of Pd and Cd and the application of Pd and Cd LIP for efficient HHG. We use different sources to demonstrate HHG from the fixed wavelength lasers and tunable lasers. We also analyze the opportunity for the resonance enhancement of a single harmonic in these two LIPs. The parametric processes during the interaction of incommensurate waves in Pd and Cd plasmas allow the generation of a broader range of harmonics, sum, and difference frequencies. We also present the theoretical consideration of TCP for harmonics generation in those plasmas.

2. Experimental

Two targets (Pd and Cd $5 \times 5 \times 2$ mm³ plates) were used for plasma formation (Fig. 1). Plasmas from Pd and Cd targets were produced in a vacuum chamber by the fundamental radiation of picosecond Nd:YAG laser (150 ps, 1064 nm, EKSPLA SL 312) using the fluence up to $F = 16$ J cm⁻². Heating pulses at $\lambda = 1064$ nm and energy up to $E_{HP} = 10$ mJ were focused using the 300 mm focal length lens. The time-resolved intensified charge-coupled device (iCCD) camera was used for the analysis of the spatial spreading of Pd and Cd plasma plumes at different moments from the beginning of ablation.

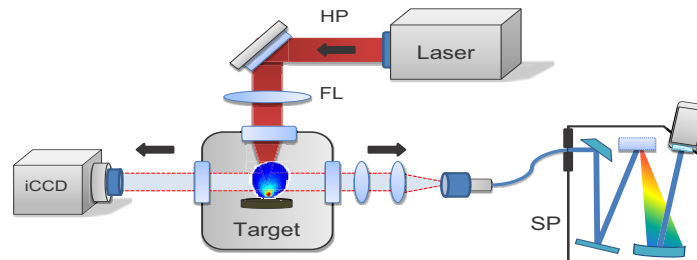


Fig. 1. Schematic of spectral and spatial measurements of plasma. HP: heating pulses (at 1064 nm), FL: focusing lens ($f = 300$ mm), Laser: picosecond laser (1064 nm, 150 ps), Target: Cd and Pd plates, iCCD: time-resolved intensified CCD camera, SP: spectrometer (Andor Kymera 328i-B1/iStar).

Ti: sapphire laser producing the 800 nm, 65 fs, 10 Hz driving pulses was used for the SCP of Pd and Cd LIP. These driving pulses were focused using the 400 mm focal length achromatic spherical lens inside the LIP produced in the vacuum chamber (Fig. 2). The optical parametric amplifier (OPA) provided the tunable 70 fs pulses in the near-infrared (NIR, 1200–1600 nm) spectral range, which also used as the driving pulses for HHG. The 3×10^{14} W cm⁻² intensity of driving pulses was used for HHG. We also used TCP of Pd and Cd LIPs. The second harmonic (H2) generation of the signal pulses of tunable OPA was used to apply the TCP scheme (NIR + H2) for plasma HHG. The conversion efficiency of H2 pulses was $\sim 14\%$.

To ablate targets, the 800 nm, 250 ps and 1064 nm, 70 ps heating pulses were used at the delay between heating and driving pulses varying in the range of 30–100 ns. In both cases, the focal spot diameter of heating radiation at the target surfaces was adjusted to be 300 μ m, and

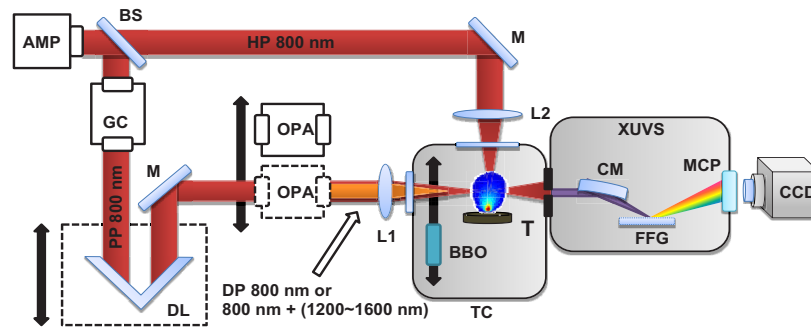


Fig. 2. Schematic of harmonics generation in Pd and Cd plasmas. AMP: uncompressed laser pulse amplifier, GC: grating compressor, BS: beam splitter, M: mirrors, L1 and L2: focusing lenses for driving pulses (DP) and uncompressed heating pulses (HP), PP 800 nm: pumping pulse for optical parametric amplifier (OPA), DL: optical delay line, TC: target chamber, BBO: barium borate crystal for second harmonic generation, XUVS: XUV spectrometer, T: target, CM: cylindrical mirror, FFG: flat-field grating, MCP: microchannel plate, CCD: charge-coupled device camera.

the intensity of heating pulses was varied between 2.3×10^{10} and 1.3×10^{11} W cm⁻². The XUV spectrometer was used for the analysis of HHG spectra [55].

3. Results

3.1. Plasma characterization

The optimized delay between two pulses and optimized heating pulse fluence are key assets ensuring efficient HHG in plasmas. The HHG efficiency strongly depends on the delay between heating and driving pulses. The heating pulse fluence variations allow determining the conditions when the influence of free electrons does not decrease the yield of harmonics. The raw images of plasma spreading at 3.7×10^4 and 5.1×10^4 m sec⁻¹ velocities out from the Pd and Cd targets, respectively, are shown in Fig. 3.

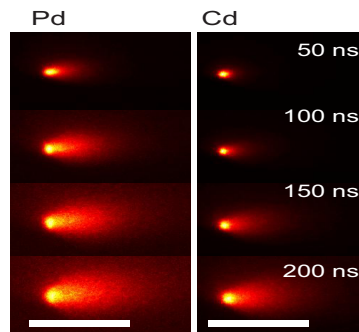


Fig. 3. The spreading of Pd and Cd plasmas at different delays between heating and driving pulses varying between 50 and 200 ns. The length of the white scale is 10 mm.

The phase-matching conditions depend on the plasma dispersion caused by the presence of the free electrons. To determine the concentration of free electrons and electron temperatures in Cd and Pd LIPs, we analyzed the spectra of two plasmas in the UV range (Figs. 4 and 5). The electron temperatures T_e were determined from five Pd I lines (324.26–360.95 nm) and six Cd I

and Cd II lines (441.56–537.8 nm) [56]. In the case of Cd, the 508.6 nm spectral line (Fig. 5(b)) was used to deduce the electron density n_e from the Stark broadening of the width of isolated spectral lines [57]. For Pd plasma, due to the unavailability of Stark broadening parameters for spectral lines in literature, only evolution of the electron temperature was presented (Fig. 4(a)). Notice that, in [58], the employment of the H_α line method allowed estimating n_e in Pd LIP to be in the range of 0.5×10^{17} and $1.0 \times 10^{17} \text{ cm}^{-3}$ for fluencies varying from $F = 10 \text{ J cm}^{-2}$ to $F = 20 \text{ J cm}^{-2}$ in the case of 20 ns heating pulses.

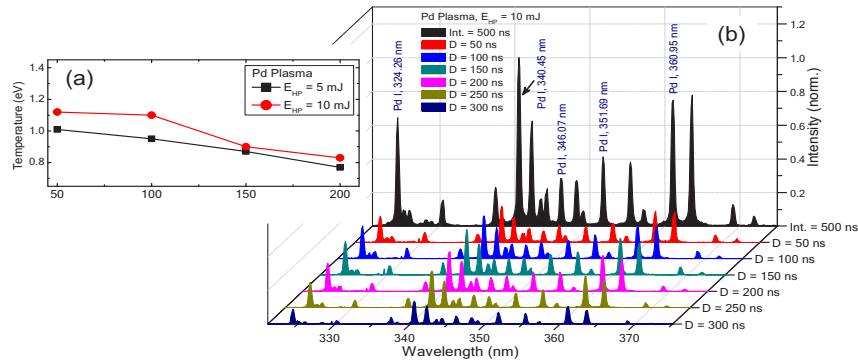


Fig. 4. (a) Calculated electron temperatures (T_e) of the Pd LIP at different delays from the beginning of ablation by 5 and 10 mJ ($F = 8 \text{ J cm}^{-2}$ and $F = 16 \text{ J cm}^{-2}$), 150 ps pulses. (b) A time-resolved spectrum of Pd plasma in the 300–380 nm range at different delays (D) from the beginning of ablation.

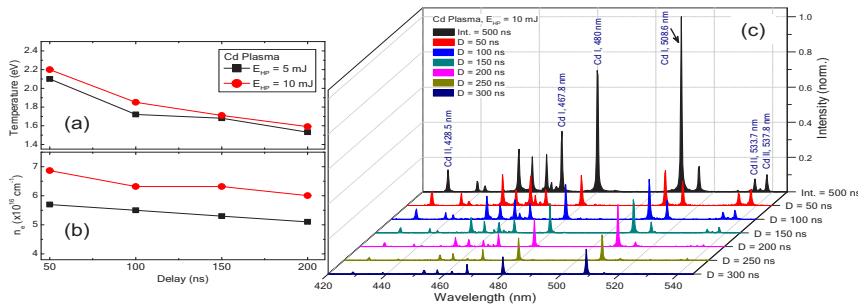


Fig. 5. (a,b) Calculated electron temperatures (T_e , in eV) and electron densities (n_e , in cm^{-3}) of Cd LIP at different delays from the beginning of ablation by 5 and 10 mJ (8 J cm^{-2} and 16 J cm^{-2}), 150 ps pulses. (c) Time-resolved spectra of Cd plasma in the 420–550 nm range at different delays (D) from the beginning of ablation.

During HHG experiments with Cd and Pd LIPs the delay was established in the range of 30–100 ns. T_{he} curves in this range of delay variations demonstrated the slow decay thus keeping the phase-matching conditions almost unchanged. One can expect a similar behavior for the small variations of n_e (Fig. 5(b)). Based on calculations of T_e and n_e for the initial period of LIP formation (up to 200 ns), one can suggest a weaker influence of the variation of those parameters on the phase-matching conditions. Correspondingly, the plasma density variation due to the expansion of LIP is expected to be the main factor influencing the harmonic generation efficiency.

Figures 6 and 7 show the integrated spectra of Pd and Cd obtained during ablation in atmospheric conditions using the fluencies 3.5 J cm^{-2} ($E = 600 \mu\text{J}$), 7 J cm^{-2} ($E = 1200 \mu\text{J}$), and 12 J cm^{-2} ($E = 2200 \mu\text{J}$) of 1064 nm heating pulses (upper panels) and 7 J cm^{-2} ($E = 300 \mu\text{J}$), and

12 J cm^{-2} ($E = 550 \mu\text{J}$) of 532 nm heating pulses (bottom panels). For Pd plasma, both at vacuum and air conditions of ablation, only strong neutral Pd I lines were observed in the studied spectral range. In contrast, the Cd plasma emitted strong Cd II lines, except for the spectra obtained using 532 nm heating pulses.

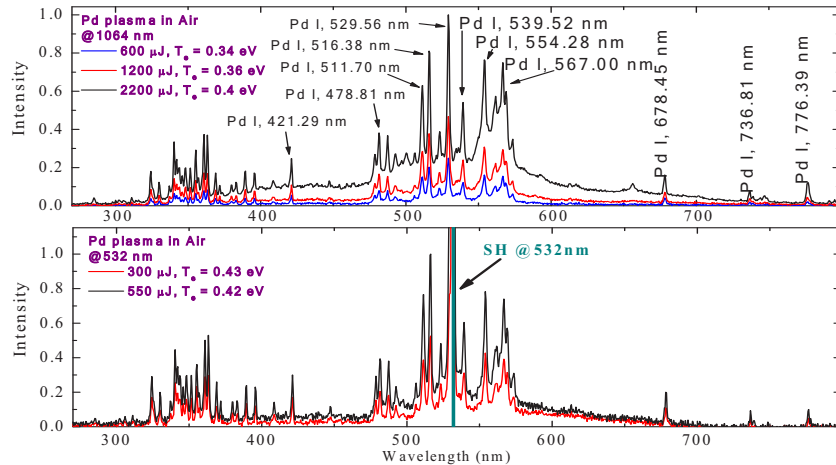


Fig. 6. Spectra of palladium plasma in the 270–800 nm range at different wavelengths and energies of the heating pulses. Upper panel: plasma was formed on the surface of bulk Pd using 1064 nm, 50 ps laser pulses. The spectra were obtained using 600 μJ (blue curve), 1200 μJ (red curve), and 2200 μJ (black curve) pulses. Bottom panel: plasma was formed on the surface of bulk Pd using 532 nm, 50 ps laser pulses. The spectra were obtained using 300 μJ (red curve) and 550 μJ (black curve) pulses.

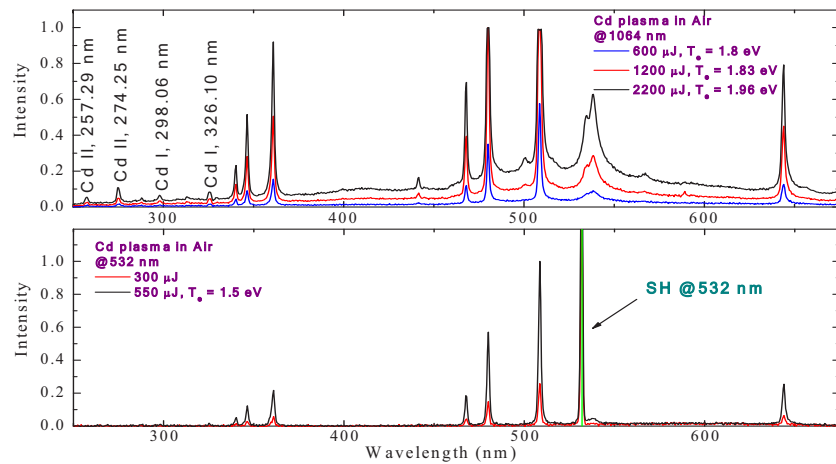


Fig. 7. Spectra of cadmium plasma in the 250–675 nm range at different wavelengths and energies of the heating pulses. Upper panel: plasma was formed on the surface of bulk Cd using 1064 nm, 50 ps laser pulses. The spectra were obtained using 600 μJ (blue curve), 1200 μJ (red curve), and 2200 μJ (black curve) pulses. Bottom panel: plasma was formed on the surface of bulk Cd using 532 nm, 50 ps laser pulses. The spectra were obtained using 300 μJ (red curve) and 550 μJ (black curve) pulses.

3.2. Calculations of the two-color pump-induced spectra of harmonics

Here we present the numerical calculations based on the strong field approximation model for the two waves interacting in the medium commonly referred to as the Lewenstein HHG model [59]. The details of calculations in the case of commensurate waves of fundamental radiation and its second harmonic can be found in [60]. Below we analyze the case when the second wave is considered incommensurate to the first wave. Notice that both metals have almost similar ionization energies (8.36 eV for Pd and 8.99 eV for Cd). Thus the calculations deduce common features of generating harmonics from two plasmas.

Contrary to the case of commensurate waves [60], the time periodicity of moment components in the case of the incommensurate frequencies is broken. Each dipole component is calculated numerically for rectangular laser pulses with a pulse duration of 65 fs. For example, in the case of 1310 nm, it gives approximately 15 optical cycles. The results of calculations of the Pd and Cd harmonic spectra are presented in Figs. 8 and 9, respectively. In the case of palladium-containing plasma, for all pump color variations the atomic system was taken as a hydrogen-like wave function with energy equal to the second ionization energy of the Pd atom (19.44 eV).

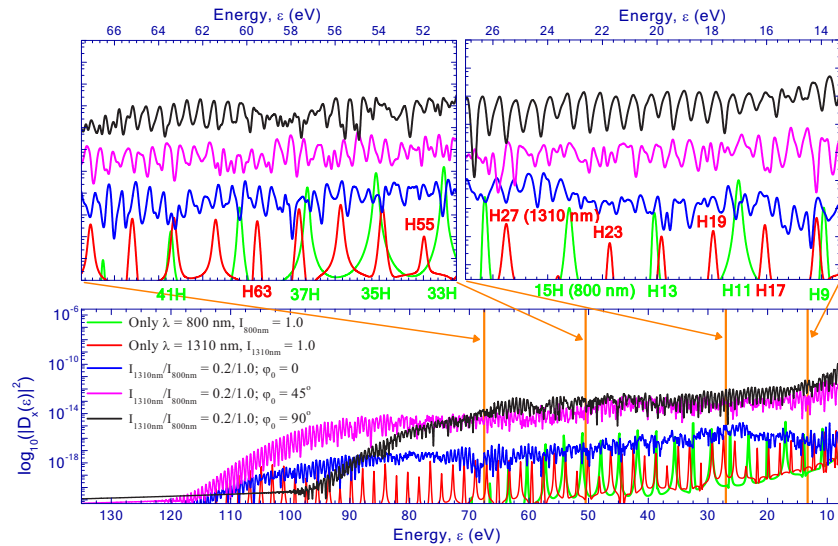


Fig. 8. Calculated HHG spectra for the parallel polarized two-color pump with $\lambda_1 = 800$ nm and $\lambda_2 = 1310$ nm. The ratio of intensities $I_{800\text{nm}}/I_{1310\text{nm}} = 1.0$. $I_{800\text{nm}} = 2.0 \times 10^{14}$ Wcm $^{-2}$. φ_0 designates a relative phase shift between the λ_1 and λ_2 fields. The top panels present the enlarged parts of the spectrum shown in the bottom panel. Red and green colored labels show the harmonic orders for the 1310 nm and 800 nm fields respectively.

The green and red profiles in Fig. 8 correspond to the harmonics from solely 800 nm and 1310 nm pumps. The intensities of those pumps were equal to each other (2.0×10^{14} Wcm $^{-2}$). The positions of cutoff harmonics were 33 H (51 eV) and 107 H (101 eV). The blue profile shows a spectrum for the two-color (800 nm + 1310 nm) pump. The intensities for that case were taken as $I_{1310\text{nm}}/I_{800\text{nm}} = 0.2/1.0$. The polarization vector directions of incommensurate pumping fields were parallel for all spectra shown in Fig. 8.

The addition of 20% intensity of the 1310 nm field to the 800 nm field led to the notable cutoff extension (from 51 eV to the region above 100 eV). The variation of phase shift φ_0 led to variations of both cutoff and harmonics enhancement, as can be seen for $\varphi_0 = 45^\circ$ and $\varphi_0 = 90^\circ$ (pink and black profiles in Fig. 8). Mixing of two incommensurate frequencies produces many additional frequency components. The intervals between them are expressed as combinations of

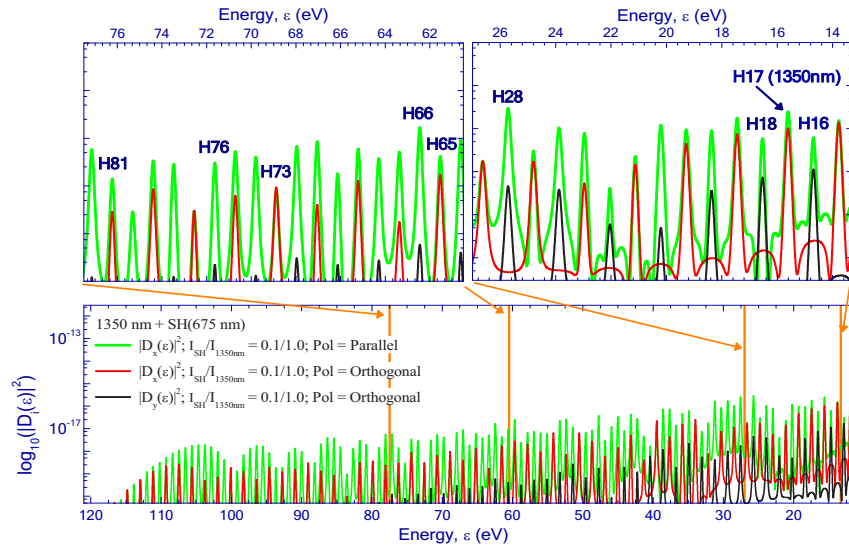


Fig. 9. The calculated HHG spectra for parallel and orthogonal two-color pumps with $\lambda_1 = 1350$ nm and $\lambda_2 = 675$ nm. The intensity $I_{1350\text{nm}}$ corresponds to 2.0×10^{14} W cm $^{-2}$. The green profiles present the harmonics for parallel orientation of 1350 nm/SH pumps, and the red and black profiles present the harmonics from orthogonal components. The top panels present the enlarged parts of the bottom spectrum. Dark blue labels show the odd and even harmonic orders of the 1350 nm pump.

$n\omega_1 \pm k\omega_2$, where the selection rule for n and k is such that the sum/difference components are multiple to $(\omega_1 + \omega_2)/4$.

In the case of the combination of fundamental and second harmonic frequencies the distribution of generated harmonics is different. The simulations for 1350 nm and its second harmonic (675 nm) are presented in Fig. 9. In that case, both parallel and orthogonal polarization orientations are presented. The intensity $I_{1350\text{nm}} = 1.0$ corresponds to 2×10^{14} Wcm $^{-2}$. The intensity of the second harmonic is taken as 10% of the intensity of the fundamental field. In contrast to incommensurate frequencies, only odd and even harmonics of the 1350 nm pump are presented.

The green profile shows the harmonics spectra for parallel orientation where mixing with a weaker second harmonic field leads to insignificant cutoff extension (from H103 to H115). The calculations for orthogonal polarizations are shown with red and black profiles. Red profiles show the spectra of the Fourier component $D_x(\varepsilon)$. The direction of this component coincides with the fundamental 1350 nm linearly polarized field. Black profiles are the spectra of $D_y(\varepsilon)$ component, corresponding to the polarization direction of the second harmonic. The spectra of $D_x(\varepsilon)$ contain only odd harmonics while the even order harmonics are emerged only from $D_y(\varepsilon)$. Similarly to the incommensurate waves, the weak contribution from the second pump leads to cutoff extension, while for the orthogonal two-color pump, the cutoff for even order harmonics is sufficiently shorter (see the red and black profiles in Fig. 9).

3.3. Harmonics generation in palladium plasma

The only report on HHG in Pd-contained LIP revealed the opportunity in the generation of harmonics up to the 25th order of 800 nm driving wave (H25, [61]). Those studies used palladium nanoparticles as the emitters of harmonics. In the present studies, we observed a stable generation of harmonics from the Pd plasma produced on the surface of the bulk target and comprised of neutrals and singly charged ions.

In the case of 800 nm driving pulses, the harmonics up to the 31st order ($E_c = 48$ eV) were observed at the optimal ablation of the bulk target. The maximal generating harmonic order increased up to H53 ($E_c \approx 49$ eV) in the case of the longer-wavelength laser source (1350 nm, Fig. 10(a)). One can see a featureless decay of harmonic yield for each next order of generating emission. The harmonic intensity (I_h) in that case was smaller compared with the application of shorter-wavelength driving pulses (800 nm) at similar intensities of 1350 and 800 nm pulses in the plasma area, which corroborates with the $I_h \propto \lambda^{-5}$ rule [62].

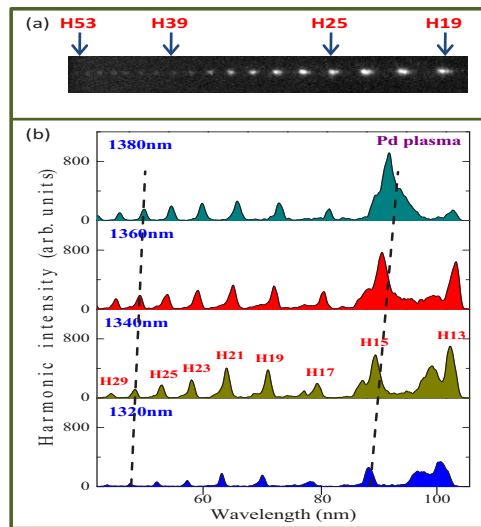


Fig. 10. (a) Raw image of harmonics distribution from Pd plasma using 1350 nm driving pulses. (b) Harmonics distributions during tuning of a single-color pump in the near-infrared region. The dashed lines show the tuning of H15 and H27.

The characteristic peculiarity of the harmonic spectrum from the ablation of bulk palladium was the appearance of the short-wavelength lobes visible in the case of lower-order harmonics, though this feature was also observed for higher-order harmonics (Fig. 10(b)). This feature dominated the emission spectra at the conditions of stronger ablation of the target (i.e. at the fluency of $F \approx 1.2$ J cm⁻²) leading in some cases to higher conversion efficiency. Note a difference in the maximum intensities of these lobes compared with the intensities of neighboring harmonics. The shifts of lobes from the harmonic wavelengths varied depending on the driving pulse intensity and the conditions of ablation. Particularly, the shorter-wavelength lobes of harmonics were not observed at weaker ($F = 0.9$ J cm⁻²) excitation of the palladium target.

Different fluencies of heating pulses on the Pd target allowed the formation of the LIPs containing various species (i.e., excited neutrals, singly and doubly charged ions, and electrons). The dynamics of HHG spectra from at weak, medium, and strong ablation refers to the conditions of plasma when harmonics are not canceled by a large density of free electrons leading to the phase mismatch between laser and harmonic waves but rather influenced by the presence of different species in the plasma. Plasma excitation was controlled by analyzing the emission spectra in the XUV range. At weak ablation of the target (i.e., at $F = 0.8$ J cm⁻²), no XUV emission lines of LIP were observed along with the harmonic spectra. A set of harmonic spectra measured using the tuning of NIR pulses with a step of 20 nm (Fig. 10(b)) was obtained at larger fluency ($F \approx 1.2$ J cm⁻²). As was mentioned, HHG spectra demonstrated the featureless pattern when each next (odd and even) order gradually decreased starting from the longest-wavelength observable harmonic up to the cut-off region. The growth of fluency led to the appearance of the

emission of excited neutral and singly charged palladium ions. However, under these conditions, the harmonics still appeared in the XUV range. Further growth of fluency (1.8 J cm^{-2}) led to the deterioration of the conditions of harmonics generation due to a large number of free electrons appearing inside the plasma volume.

The estimated plasma density ($1 \times 10^{17} \text{ cm}^{-3}$) was not as high as the one at which the appearance of the phase mismatch between interacting waves caused by ionization of plasma particles becomes the main restricting factor of HHG. To keep these conditions we maintained the optimal ablation of the Pd target allowing maximum yield of harmonics at the used sizes of plasma formation (0.3 mm).

A difference in harmonic yields in the case of the NIR pulses varying between 1320 and 1380 nm is caused by the larger energy of the longer-wavelength driving pulses (Fig. 10(b)). This figure shows the variation of harmonics wavelength during tuning of a single-color pump in the near-infrared region. The dotted lines show the tuning of H15 and H27. As one can see, four harmonic spectra showed approximately similar energy distribution, which did not change during variation of the wavelength of driving pulses. Based on this observation, one can judge the absence of ionic transitions possessing large oscillator strength (gf) in the studied XUV range (47–106 nm).

Insertion of the BBO crystal on the path of the focused driving beam drastically modified the harmonic spectrum from Pd LIP. TCP using orthogonally polarized commensurate waves (NIR + H2) allowed $\sim 2\times$ to $3\times$ growth of the yield of odd harmonics, comparable harmonic intensities for the odd and even orders, and extension of the harmonic cutoff compared with the SCP. Additionally, the tuning of odd and even harmonics allowed a rather accurate analysis of the realization of the resonance-induced single harmonic generation compared with the case of SCP of Pd plasma. However, in that case, we also did not observe the enhancement of some specific odd or even harmonic using different wavelengths of driving pulses. Thus the studied plasma did not reveal the influence of the excited states on the harmonic distribution at different excitation conditions of the ablating palladium target. Notice that, in the case of Cd plasma, this approach allowed observing the single harmonic enhancement in a few spectral ranges (see next subsection).

The application of the TCP comprising incommensurate waves (tunable NIR + Ti: sapphire pulses) in the case of ablation of the bulk palladium led to the prevailing generation of harmonics from the stronger lower-wavelength component (i.e. 800 nm pulses), especially at the conditions when these two pulses showed worse overlap inside the plasma. Figure 11(a) shows the case when a relatively weak signal wave (1310 nm) interacted with the stronger 800 nm wave ($I_{1310\text{nm}}: I_{800\text{nm}} = 0.16$) in plasma at the partial overlap of these two pulses. The delay between these two pulses was 56 fs. One can see the absence of the influence of the longer-wavelength component of TCP on the harmonics distribution. Only odd harmonics of 800 nm waves were presented in this spectrum.

Better overlap of two driving pulses in Pd LIP caused a drastic change in generated XUV emission (Fig. 11(b)). The emission attributed to the combination of the frequencies of two pumps appeared between the strong odd harmonics of the 800 nm pump. This figure shows the spectrum of generated frequency components using the 1310 nm and 800 nm orthogonally polarized pulses properly overlapping with each other during propagation through the Pd plasma.

These coherent emission lines were extended below the spectral region of observation (45–105 nm) and represented two additional sum and difference frequencies between each odd harmonic originating from the stronger 800 nm pump. Notice that the intensities of these additional components were approximately 2 to 3 times smaller than the intensities of neighboring odd harmonics attributed to the 800 nm pump. Meanwhile, the ratio of the 1310 and 800 nm pumps was notably smaller (1:6). This observation points out the crucial role of the weak second

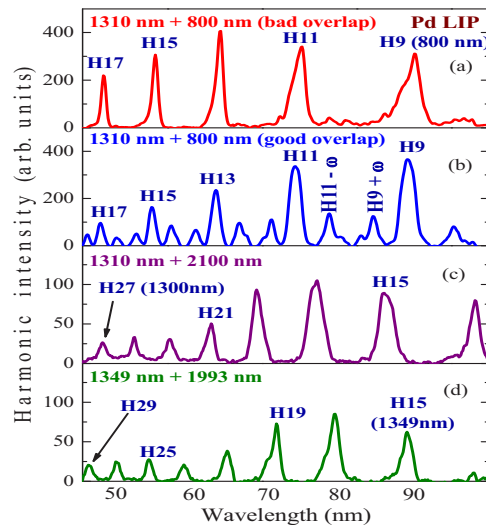


Fig. 11. Different combinations of the two-color pump of Pd plasma at variable overlaps of two waves (see text).

wave in the parametric interaction inside the plasma volume at the perfect overlap of the two waves.

We also used other configurations when two waves were taken from the same optical parametric amplifier. Instead of a strong 800 nm wave, we used the signal wave (1300 nm, Fig. 11(c) and 1349, Fig. 11(d)), while the second waves were idler pulses ($\lambda = 2100$ nm and 1993 nm, respectively). At these conditions, we did not observe the parametric process of sum and difference frequencies generation but rather obtained the odd harmonics from the stronger (1310 and 1349 nm) despite the perfect overlap of two idler waves (2100 nm, Fig. 11(c) and 1993 nm, Fig. 11(d)) with corresponding 1300 and 1349 nm signal waves. The ratio of pulse energies of strong and weak waves in these experiments was $\sim 20:1$. Taking into account the $I_h \propto \lambda^{-5}$ rule one can expect the lesser influence of notably weaker waves on the process of sum and difference frequencies generation. Thus, only relatively strong 1310 and 1349 nm waves participated in the generation of odd harmonics.

3.4. Harmonics emission from cadmium plasma

Similarly to the palladium plasma, we conducted the HHG in Cd LIP. To the best of our knowledge, this plasma was not considered and analyzed previously as an example of an efficient medium for HHG. The optimization of this plasma for efficient harmonics generation was the same as for Pd LIP. At high fluency of picosecond heating pulses ($F = 2.9$ J cm $^{-2}$), only plasma emission dominated the XUV spectra.

The upper panel of Fig. 12 shows the raw image of plasma emission and relative intensities of ionic transitions. The calibration using the NIST database [63] showed that, at this level of target excitation, the dominating transitions in the 45–100 nm range were those attributed to Cd II – Cd IV ions. No harmonics were observed during the propagation of driving pulses through such plasma due to a strong phase mismatch between the fundamental and harmonic waves caused by a large concentration of free electrons.

The application of twice smaller fluence ($F = 1.4$ J cm $^{-2}$) led to the disappearance of plasma emission and the formation of the optimal plasma conditions for harmonics generation. The gradually decreased odd harmonics of 800 nm radiation were achieved in the case of SCP, though

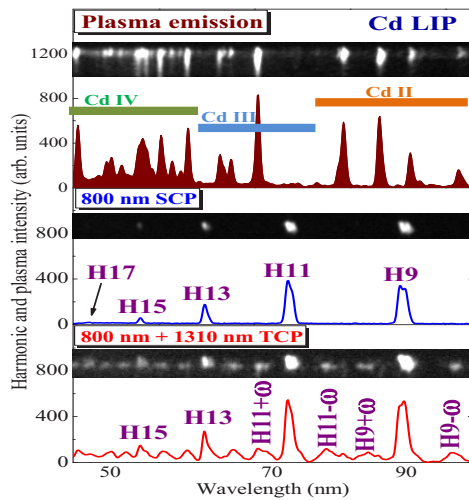


Fig. 12. Plasma emission in XUV (upper panel), HHG from 800 nm SCP (middle panel), and parametric waves generation from 800 nm + 1310 nm TCP of Cd plasma (bottom panel, see text). Raw images show the plasma and coherent emission distributions along the 46–100 nm spectral range.

the cutoff harmonic, in that case, was relatively small (H27; see raw image of XUV spectrum and intensity distribution of harmonics in the middle panel of Fig. 12). The application of TCP using the incommensurate waves (800 nm and 1310 nm) perfectly overlapping in the plasma area allowed achieving generation of sum and difference harmonics ($H_{800\text{nm}} \pm \omega_{1310\text{nm}}$). The bottom panel of Fig. 12 shows the raw image of the generated spectrum of odd harmonics and sum/difference frequencies. This process was similar to the one described in the case of Pd plasma, though the generation of $H_{800\text{nm}} \pm \omega_{1310\text{nm}}$ parametric waves in cadmium plasma was less efficient compared with the Pd LIP.

The next stage of the TCP of Cd LIP was based on the application of the tunable near-infrared pulses from the optical parametric amplifier combined with the second harmonic of those pulses. The higher conversion efficiency into the second harmonic wave in the case of the NIR region allows for the experimental study of TCP HHG at comparable intensities of the driving field components. The goal of these studies was to determine the XUV region allowing observation of the resonantly-enhanced harmonic, similar to the studies of Pd LIP (Fig. 10(b)).

Figure 13 shows the set of harmonic spectra obtained using different driving pulses and their second harmonics. The tuning of NIR pulses was performed between 1290 and 1410 nm with the step of 20 nm. The dashed lines show the tuning of H13 – H15 harmonics. This range of harmonics wavelength variations allowed tuning of the n^{th} order towards the $(n + 1)^{\text{th}}$ order. We observed two regions (in the vicinity of 81.7 and 88.4 nm) marked in this figure by black arrows at which the nearby harmonics become enhanced with regard to the neighbor harmonic orders. Though the resonance-induced enhancement factor at these wavelengths was relatively small ($\sim 2\times$), this observation demonstrates the presence of some ionic transitions possessing relatively large gfs .

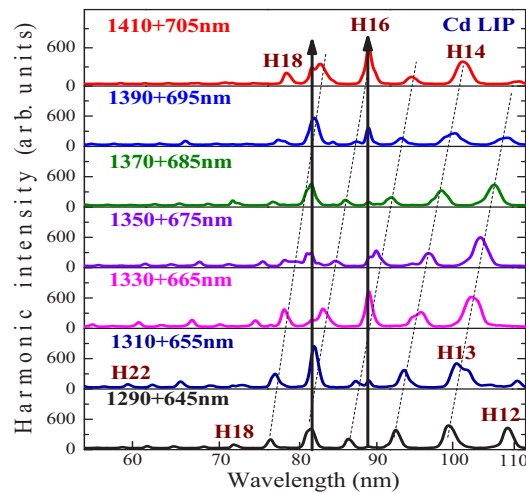


Fig. 13. Harmonic spectra obtained from Cd LIP using different combinations of driving pulses and their second harmonics. The tuning of NIR pulses was performed between 1290 and 1410 nm with the step of 20 nm. The dashed lines show the tuning of H13 – H15 harmonics. The arrows show the wavelengths at which some resonance-induced enhancement of nearby coherent emission was observed.

4. Discussion

As it was mentioned, the choice of the studied samples (palladium and cadmium) was based on the analysis of the metal elements belonging to the fifth period of periodic table, which previously have been recognized as the targets for the optimal laser-induced plasma formation resulting in the best conditions for harmonics generation. We assumed that two other metals of the fifth period of the table (Pd and Cd) could also be treated as the perspective plasma media for HHG.

The presented results comprise various aspects, which have distinctions compared with the harmonics generation in gases and previous reports on harmonics generation in LIPs. The analysis of plasmas characteristics, the dynamics of LIPs spreading, the visible and XUV spectral features of plasmas, the application of the single-color and two-color pumps in different configurations, the observation of the resonance enhancement of single harmonic in Cd plasma, the theoretical calculations of harmonic spectra, sum and difference frequencies generation in the XUV range, the spectral tuning of harmonics, the comparative analysis of HHG using shorter- and longer-wavelength driving sources, and the observation of two regions (in the vicinity of 81.7 and 88.4 nm) at which the nearby harmonics becomes enhanced with regard to the neighbor harmonic orders in the case of Cd plasma comprise the studies carried out in a single set using the cadmium and palladium LIPs. Among the novelties, we would like to mention the first demonstration of the dual enhancement of harmonic in different XUV ranges, which is a peculiarity of the cadmium plasma (Fig. 13). The targets (Pd, Cd) used for plasma formation were applied for HHG for the first time. This study can be considered an example of material science through the analysis of the nonlinear optical response of the Pd and Cd plasmas.

An atom or a molecule can absorb light and undergo a transition from one quantum state to another. The oscillator strength of a transition from a lower state to an upper state, f , is a key parameter in the description of the line absorption coefficient. Although the f -value is an indicator of line strength, it is often presented weighted by the statistical weight, g , of the level from which the transition originates. The gf -value is therefore expected to be larger when there are fewer decay channels. In general, oscillator strength is a dimensionless quantity that expresses

the probability of absorption or emission of electromagnetic radiation in transitions between energy levels of an atom or molecule. For example, if an emissive state has a small oscillator strength, nonradiative decay will outpace radiative decay. Conversely, “bright” transitions will have large oscillator strengths (compare the upper panel of Fig. 12 and the enhancement of harmonics in the vicinity of 82 and 88 nm in the case of cadmium plasma). The oscillator strength can be thought of as the ratio between the quantum mechanical transition rate and the classical absorption/emission rate of a single electron oscillator with the same frequency as the transition.

As for the topics of the present study, the question arises as to whether can we obtain a strong enhancement of a single harmonic within the harmonic spectrum in the case when this harmonic becomes close to the ionic transitions of Cd and Pd possessing relatively large oscillator strength. Earlier, this issue was analyzed during a few studies demonstrating strong enhancement of a single harmonic in some laser-induced plasmas (in particular, In, Sn, Cr, Mn). Notice that no similar effect was reported in the case of HHG in gases. Meanwhile, starting from the first observation of this effect in indium plasma [64], the role of the ionic transitions possessing large values of gf in the formation of the conditions for the enhancement of a single harmonic was discussed in the community. The comparison with a past study on In plasma emission [65] showed that most of the indium plasma emission is due to radiative transitions to the ground state and the low-lying state of In II. The gf of one of those transitions has been calculated to be 1.11, which is more than 12 times larger than other transitions from the ground state of In II. This transition can be driven into resonance with the 13th harmonics (61.2 nm, 20.26 eV) of 800 nm laser by the AC-Stark shift, thereby resonantly enhancing its intensity.

Such intensity enhancement can be attributed to the existence of oscillating electron trajectories that revisit the origin twice per laser cycle. Since such trajectories start from the resonantly populated excited state, with a nonzero initial kinetic energy, they still have nonzero instantaneous kinetic energies when they return to the origin. As usual, recombination results in the emission of harmonics, but due to the relatively low probabilities, the population in the laser-driven wave packets increases continuously and the probability for harmonic emission grows with the number of allowed recollisions. These multiple recollisions are predicted to enhance harmonics under atomic resonance [64].

To determine the applicability of the $I_h \propto \lambda^{-5}$ rule to the ionic plasma one has to compare the harmonics at similar intensities of the driving pulses (800 and 1350 nm). In our case, the harmonic yield from Pd plasma using NIR pulses (1350 nm) was significantly weaker than in the case of the 800 nm pump. The comparison of these two pumps at similar energy pulses (1 mJ) showed a seven-fold decrease of harmonic yield from the palladium plasma in the case of the 1350 nm pulses compared with the 800 nm pulses, which was slightly below the theoretical prediction of the ratio $(\lambda_{800 \text{ nm}} / \lambda_{1350 \text{ nm}})^{-5} \approx 11.8$. Various processes could cause this deviation from the above rule, such as the self-phase modulation, some difference in peak intensity caused, particularly, by a difference in pulse duration and heterogeneity in the focal plane, involvement of different emitters for HHG, etc.

Most of our experiments using the radiation from OPA were carried out using the TCP of plasmas. The reasons for using the TCP instead of a single-color pump were related to the small energy of signal pulses. As it was mentioned, the $I_h \propto \lambda^{-5}$ rule led to a significant decrease of odd harmonics yield in the case of the weaker longer-wavelength sources compared with the stronger 800 nm pump. Because of this, we used the second harmonic generation of signal pulses to apply the TCP scheme (NIR + H2) for plasma HHG.

Meanwhile, in the case of Pd plasma, the comparison of TCP during our attempts to generate sum and difference frequencies was carried out using the NIR pulses of different wavelengths produced in OPA (Figs. 11(c) and 11(d)). The $I_h \propto \lambda^{-5}$ rule was applied to these TCP studies from the point of view of the relative role of signal (1310 nm) and idler (2100 nm) waves in the sum and difference frequencies generation. Apart from the larger intensity of the signal wave

compared with the idler one, the above rule allows for a comparison of the ratio of harmonic yields from these sources as $I_H(1310\text{ nm})/I_H(2300\text{ nm}) \propto (1310/2300)^{-5} \approx 17$, at equal intensities of those waves. Correspondingly, the role of the second wave (2100 nm) in these sum/difference frequencies experiments was insignificant, which resulted in the generation of only odd harmonics of the signal waves in the palladium plasma during these TCP experiments (Fig. 11(c)). The same was true for the pair of 1349 nm and 1993 nm waves (Fig. 11(d)).

We tried to find an influence of the plasma conditions on the generation of sum and difference frequencies in the harmonic spectra and did not reveal such a relationship. The formation of the low-density plasma comprising neutrals, singly-charged ions, and electrons was treated from the point of view of the creation of the most suitable conditions for HHG (i.e. largest harmonic yield, highest cutoff, etc.). Meanwhile, the generation of the sum and difference frequencies was mostly related to technical issues like the spatiotemporal overlap of the pumping waves in the plasma area, relative intensities of the signal and idler pumps from OPA, as well as their relation with regard to the intensity of the 800 nm pump.

5. Conclusions

In conclusion, we have described the studies of plasma formation during laser ablation of Pd and Cd with further application of these two laser-induced plasmas for the high-order harmonics generation of ultrashort laser pulses. We studied the characteristics of two plasmas and determined the plasma velocities, electron temperatures, and electron densities. Different laser sources were used to demonstrate HHG from the fixed wavelength sources and tunable sources of laser light. We have also analyzed the opportunity for resonance enhancement of single harmonic in these two plasmas. The application of a two-color pump of Pd and Cd plasmas using commensurate waves (driving beam and its second harmonic) and incommensurate waves (800 nm wave and signal beams from optical parametric amplifier) led to the enhancement of harmonic yield. It was demonstrated that the parametric processes during the interaction of incommensurate waves in Pd and Cd plasmas allow the generation of a broader range of harmonics. We also presented the theoretical consideration of the two-color pump of laser-induced plasma.

Funding. European Regional Development Fund (1.1.1.5/19/A/003); World Bank Project (REP-04032022-206).

Acknowledgments. R.A.G. is grateful to H. Kuroda for providing access to the laser facility. Institute of Solid State Physics, University of Latvia as the Center of Excellence has received funding from the European Union's Horizon 2020 Framework Programme H2020-WIDESPREAD-01-2016-2017-TeamingPhase2 under grant agreement No. 739508, project CAMART².

Disclosures. The authors declare no conflict of interest

Data availability. The data that support the findings of this study are available on request from the corresponding author.

References

1. N. Kanda, T. Imahoko, K. Yoshida, A. Tanabashi, A. A. Eilanlou, Y. Nabekawa, T. Sumiyoshi, M. Kuwata-Gonokami, and K. Midorikawa, "Opening a new route to multipoint coherent XUV sources via intracavity high-order harmonic generation," *Light: Sci. Appl.* **9**(1), 168 (2020).
2. S. Hädrich, M. Krebs, A. Hoffmann, A. A. Klenke, J. Rothhardt, J. Limpert, and A. Tünnermann, "Exploring new avenues in high repetition rate table-top coherent extreme ultraviolet sources," *Light: Sci. Appl.* **4**(8), e320 (2015).
3. M. Gebhardt, T. Heuermann, R. Klas, C. Liu, A. Kirsche, M. Lenski, Z. Wang, C. Gaida, J. E. Antonio-Lopez, A. Schülzgen, R. Amezcua-Correa, J. Rothhardt, and J. Limpert, "Bright, high-repetition-rate water window soft X-ray source enabled by nonlinear pulse self-compression in an antiresonant hollow-core fibre," *Light: Sci. Appl.* **10**(1), 36 (2021).
4. S. Witte, V. Tenner, D. W. E. Noom, and K. S. E. Eikema, "Lensless diffractive imaging with ultra-broadband table-top sources: from infrared to extreme-ultraviolet wavelengths," *Light: Sci. Appl.* **3**(3), e163 (2014).
5. F. Tuitje, P. Martínez Gil, T. Helk, J. Gautier, F. Tissandier, J.-P. Goddet, A. Guggenmos, U. Kleineberg, S. Sebban, E. Oliva, C. Spielmann, and M. Züch, "Nonlinear ionization dynamics of hot dense plasma observed in a laser-plasma amplifier," *Light: Sci. Appl.* **9**(1), 187 (2020).

6. Z. Wang, H. Park, Y. H. Lai, J. Xu, C. I. Blaga, F. Yang, P. Agostini, and L. F. DiMauro, "The roles of photo-carrier doping and driving wavelength in high harmonic generation from a semiconductor," *Nat. Commun.* **8**(1), 1686 (2017).
7. S. Li, Y. Tang, L. Ortmann, B. K. Talbert, C. I. Blaga, Y. H. Lai, Z. Wang, Y. Cheng, F. Yang, A. S. Landsman, P. Agostini, and L. F. DiMauro, "High-order harmonic generation from a thin film crystal perturbed by a quasi-static terahertz field," *Nat. Commun.* **14**(1), 2603 (2023).
8. Y. H. Lai, K. S. Rao, J. Liang, X. Wang, C. Guo, W. Yu, and W. Li, "Resonance-enhanced high harmonic in metal ions driven by elliptically polarized laser pulses," *Opt. Lett.* **46**(10), 2372–2375 (2021).
9. W. Fu, J. Wang, J. Yu, and W. Li, "Extension of high-order harmonic generation cutoff from laser-ablated tin plasma plumes," *Opt. Express* **31**(10), 15553–15563 (2023).
10. W. Fu, Y. H. Lai, and W. Li, "Comparative study of medium length-dependent high-harmonic generation from metal ions," *Opt. Express* **30**(26), 47315–47325 (2022).
11. B. Dromey, M. Zepf, A. Gopal, K. Lancaster, M. S. Wei, K. Krushelnick, M. Tatarakis, N. Vakakis, S. Moustazis, R. Kodama, M. Tambo, C. Stoeckl, R. Clarke, H. Habara, D. Neely, S. Karsch, and P. Norreys, "High harmonic generation in the relativistic limit," *Nat. Phys.* **2**(7), 456–459 (2006).
12. F. Quéré, C. Thauray, P. Monot, S. Dobosz, P. Martin, J.-P. Geindre, and P. Audebert, "Coherent wake emission of high-order harmonics from overdense plasmas," *Phys. Rev. Lett.* **96**(12), 125004 (2006).
13. C. Thauray, F. Quéré, J.-P. Geindre, A. Levy, T. Ceccotti, P. Monot, M. Bougeard, F. Rau, P. d'Oliveira, P. Audebert, R. Marjoribanks, and P. Martin, "Plasma mirrors for ultrahigh-intensity optics," *Nature Phys.* **3**(6), 424–429 (2007).
14. G. S. Boltaev, R. A. Ganeev, V. V. Kim, and A. S. Alnaser, "High-harmonic generation in the lanthanides-containing plasmas," *AIP Adv.* **10**(1), 015231 (2020).
15. M. Iqbal, R. A. Ganeev, G. S. Boltaev, V. V. Kim, and A. S. Alnaser, "Incoherent and coherent extreme ultraviolet emission from boron plasma," *Eur. Phys. J. D* **74**(2), 28 (2020).
16. M. Venkatesh, R. A. Ganeev, D. S. Ivanov, G. S. Boltaev, V. V. Kim, L. Jingguang, I. N. Zavestovskaya, M. E. Garcia, and C. Guo, "High-order harmonics generation in Au nanoparticles-contained plasma," *Nanomater.* **10**(2), 234 (2020).
17. G. S. Boltaev, R. A. Ganeev, V. V. Kim, N. A. Abbasi, M. Iqbal, and A. S. Alnaser, "Comparison of the high-order harmonics generation in the plasmas produced on different rotating targets during ablation using 1 kHz and 100 kHz lasers," *Opt. Express* **28**(13), 18859–18875 (2020).
18. G. S. Boltaev, V. V. Kim, M. Iqbal, N. A. Abbasi, V. S. Yalishev, R. A. Ganeev, and A. S. Alnaser, "Application of 150 kHz laser for high-order harmonic generation in different plasmas," *Photonics* **7**(3), 66 (2020).
19. V. V. Kim, G. S. Boltaev, M. Iqbal, N. A. Abbasi, H. Al-Harmi, I. S. Wahyutama, T. Sato, K. L. Ishikawa, R. A. Ganeev, and A. S. Alnaser, "Resonance enhancement of harmonics in the vicinity of 32 nm spectral range during propagation of femtosecond pulses through the molybdenum plasma," *J. Phys. B: At. Mol. Opt. Phys.* **53**(19), 195401 (2020).
20. R. A. Ganeev, G. S. Boltaev, S. Y. Stremoukhov, V. V. Kim, A. V. Andreev, and A. S. Alnaser, "High-order harmonic generation during different overlaps of two-colored pulses in laser-produced plasmas," *Eur. Phys. J. D* **74**(10), 199 (2020).
21. J. Liang, M. Venkatesh, G. S. Boltaev, R. A. Ganeev, Y. H. Lai, and C. Guo, "Investigation of resonance-enhanced high-order harmonics by two-component laser-produced plasmas," *Atoms* **9**(1), 1 (2021).
22. R. A. Ganeev and H. Kuroda, "High-order harmonics generation in atomic and molecular zinc plasmas," *Photonics* **8**(2), 29 (2021).
23. V. V. Kim, R. A. Ganeev, G. S. Boltaev, M. Iqbal, and A. S. Alnaser, "Carbon-containing nanostructured plasma: medium for efficient high-order harmonics of 1030 nm laser," *Phys. Plasmas* **28**(2), 023111 (2021).
24. R. A. Ganeev, V. V. Kim, K. S. Rao, and C. Guo, "Probing laser plasma dynamics using high-order harmonics generation in carbon-containing nanomaterials," *Appl. Sci.* **11**(5), 2143 (2021).
25. R. A. Ganeev and H. Kuroda, "Reexamining different factors of the resonance-enhanced high-order harmonic generation in atomic and nanoparticle laser-induced tin plasmas," *Appl. Sci.* **11**(5), 2193 (2021).
26. R. A. Ganeev, G. S. Boltaev, V. V. Kim, M. Iqbal, H. Kuroda, and A. S. Alnaser, "Distinction in resonance properties of the atomic and molecular plasmas used for high-order harmonics generation of ultrafast laser pulses," *J. Appl. Phys.* **129**(4), 043103 (2021).
27. R. A. Ganeev and H. Kuroda, "Resonance-affected high-order harmonic emission from atomic and molecular chromium laser-induced plasmas," *OSA Continuum* **4**(5), 1545–1554 (2021).
28. V. V. Kim, R. A. Ganeev, K. S. Rao, W. Yu, and W. Li, "Analysis of laser plasma dynamics using the time resolved nonlinear optical response of ablated carbon nanocomposites mixed with epoxy resin," *Opt. Express* **29**(22), 35877–3590 (2021).
29. S. R. Konda, V. R. Soma, R. A. Ganeev, M. Banavoth, R. Ketavath, and W. Li, "Third-order optical nonlinearities and high-order harmonics generation in Ni-doped CsPbBr₃ nanocrystals using single- and two-color chirped pulses," *J. Mater. Sci.* **57**(5), 3468–3485 (2022).
30. M. Venkatesh, R. A. Ganeev, V. V. Kim, G. S. Boltaev, I. B. Sapaev, J. Liang, J. Yu, and W. Li, "Application of vector beams for enhanced high-order harmonics generation in laser-induced plasmas," *Opt. Express* **30**(10), 17080 (2022).

31. R. A. Ganeev, V. V. Kim, G. S. Boltaev, I. B. Sapaev, and S. Y. Stremoukhov, "Joint manifestation of quasi-phase-matching and resonance enhancement of harmonics laser-induced plasmas," *Optics Continuum* **1**(5), 1098–1116 (2022).
32. V. V. Kim, R. A. Ganeev, S. R. Konda, G. S. Boltaev, I. B. Sapaev, W. Yu, and W. Li, "High-order harmonics generation in the laser-induced lead-free perovskites-containing plasmas," *Scient. Reports* **12**(1), 9128 (2022).
33. R. A. Ganeev, "Laser-induced molecular plasma: a medium for high-order harmonics generation of ultrashort pulses," *Int. J. Mol. Sci.* **23**(14), 7613 (2022).
34. V. V. Kim, J. Butikova, J. Grube, A. Sarakovskis, and R. A. Ganeev, "Plasma dynamics characterization for improvement of resonantly-enhanced harmonics generation in indium and tin laser-produced plasmas," *Photonics* **9**(9), 600 (2022).
35. G. S. Boltaev, A. M. Abu Baker, M. Iqbal, N. Abbasi, R. A. Ganeev, and A. S. Alnaser, "Low-order nonlinearities and high-order harmonics generation in Zn and ZnSe nanoparticles synthesized during femtosecond laser ablation at 50 kHz pulse repetition rate," *J. Opt. Soc. Am. B* **39**(10), 2794–2803 (2022).
36. R. A. Ganeev, "Low- and high-order optical nonlinearities of quantum dots," *Photonics* **9**(10), 757 (2022).
37. V. V. Kim, J. Grube, J. Butikova, A. Sarakovskis, and R. A. Ganeev, "Influence of chromium plasma characteristics on high-order harmonics generation," *Appl. Phys. B* **128**(12), 217 (2022).
38. S. R. Konda, R. A. Ganeev, V. V. Kim, Y. Jiaqi, and W. Li, "High-order harmonics generation in nanosecond-pulses-induced plasma containing Ni-doped CsPbBr₃ perovskite nanocrystals using chirp-free and chirped femtosecond pulses," *Nanotechnol.* **34**(5), 055705 (2023).
39. R. A. Ganeev, "High-order harmonic generation in laser plasma: past and recent achievements," *Appl. Phys. B* **129**(1), 17 (2023).
40. S. R. Konda, R. A. Rajan, S. Singh, R. A. Ganeev, V. R. Soma, A. Srivastava, M. Venkatesh, C. Guo, and W. Li, "Influence of embedded NiO-nanoparticles on the nonlinear absorption of tungsten disulfide nanolayers," *Opt. Mater.* **138**, 113657 (2023).
41. M. Venkatesh, V. V. Kim, G. S. Boltaev, S. R. Konda, P. Svedlindh, W. Li, and R. A. Ganeev, "High-order harmonics generation in MoS₂ transition metal dichalcogenides: effect of nickel and carbon nanotube dopants," *Int. J. Mol. Sci.* **24**(7), 6540 (2023).
42. R. A. Ganeev, "Three-color pump of laser-induced plasmas: sum and difference frequencies generation," *Opt. Lett.* **48**(8), 2038–2041 (2023).
43. G. S. Boltaev, R. A. Ganeev, I. A. Shuklov, A. A. Lizunova, D. V. Dyomkin, T. Milenkovich, A. Abu Baker, and A. S. Alnaser, "Studies of the low- and high-order optical nonlinearities of mercury selenide quantum dots using femtosecond pulses," *Appl. Phys. B* **129**(6), 100 (2023).
44. L. B. Elouga Bom, F. Bouzid, F. Vidal, J. C. Kieffer, and T. Ozaki, "Correlation of plasma ion densities and phase matching with the intensities of strong single high-order harmonics," *J. Phys. B: At. Mol. Opt. Phys.* **41**(21), 215401 (2008).
45. L. B. Elouga Bom, Y. Pertot, V. R. Bhardwaj, and T. Ozaki, "Multi- μ J coherent extreme ultraviolet source generated from carbon using the plasma harmonic method," *Opt. Express* **19**(4), 3077–3085 (2011).
46. M. A. Fareed, V. V. Strelkov, N. Thire, S. Mondal, B. E. Schmidt, F. Legare, and T. Ozaki, "High-order harmonic generation from the dressed autoionizing states," *Nat. Commun.* **8**(1), 16061 (2017).
47. M. Kumar, H. Singhal, and J. A. Chakera, "High order harmonic radiation source for multicolor extreme ultraviolet radiography of carbon plumes," *J. Appl. Phys.* **125**(15), 155902 (2019).
48. M. Singh, M. A. Fareed, A. Laramée, E. Isgandarov, and T. Ozaki, "Intense vortex high-order harmonics generated from laser-ablated plume," *Appl. Phys. Lett.* **115**(23), 231105 (2019).
49. S. R. Konda, Y. H. Lai, and Y. W. Li, "Investigation of high harmonic generation from laser ablated plumes of silver," *J. Appl. Phys.* **130**(1), 013101 (2021).
50. S. R. Konda, V. R. Soma, M. Banovath, R. Ketavath, V. Mottamchetty, Y. H. Lai, and W. Li, "High harmonic generation from laser-induced plasmas of Ni-doped CsPbBr₃ nanocrystals: Implications for extreme ultraviolet light sources," *ACS Appl. Nano Mater.* **4**(8), 8292–8301 (2021).
51. R. A. Ganeev, H. Singhal, P. A. Naik, I. A. Kulagin, P. V. Redkin, J. A. Chakera, M. Tayyab, R. A. Khan, and P. D. Gupta, "Enhancement of high-order harmonic generation using two-color pump in plasma plumes," *Phys. Rev. A* **80**(3), 033845 (2009).
52. P. Lan, E. Takahashi, and K. Midorikawa, "Optimization of infrared two-color multicycle field synthesis for intense-isolated-attosecond pulse generation," *Phys. Rev. A* **82**(5), 053413 (2010).
53. R. A. Ganeev, "High-order sum and difference frequency generation using tunable two- and three-color commensurate and incommensurate mid-infrared pumps of graphite plasma," *J. Opt. Soc. Am. B* **33**(12), E93–E101 (2016).
54. E. Takahashi, P. Lan, O. D. Mücke, Y. Nabekawa, and K. Midorikawa, "Infrared two-color multicycle laser field synthesis for generating an intense attosecond pulse," *Phys. Rev. Lett.* **104**(23), 233901 (2010).
55. R. A. Ganeev, M. Suzuki, S. Yoneya, and H. Kuroda, "Resonance-enhanced harmonic generation in nanoparticle-containing plasmas," *J. Phys. B: At. Mol. Opt. Phys.* **48**(16), 165401 (2015).
56. O. Balki, M. M. Rahman, and H. E. Elsayed-Ali, "Optical emission spectroscopy of carbon laser plasma ion source," *Opt. Commun.* **412**, 134–140 (2018).
57. Z. Simić, M. S. Dimitrijević, N. Milovanović, and S. Sahal-Bréchet, "Stark broadening of Cd I spectral lines," *Astronomy & Astrophys.* **441**(1), 391–393 (2005).

58. S. A. Abbasi, Z. Aziz, T. M. Khan, D. Ali, T. ul Hassan, J. Iqbal, S. U. Khan, A. Ahmad, R. Khan, and E. M. Khan, "Enhancement of optical signal and characterization of palladium plasma by magnetic field-assisted laser-induced breakdown spectroscopy," *Optik* **224**, 165746 (2020).
59. M. Lewenstein, P. Balcou, M. Y. Ivanov, A. L'Huillier, and P. B. Corkum, "Theory of high-harmonic generation by low-frequency laser fields," *Phys. Rev. A* **49**(3), 2117–2132 (1994).
60. V. V. Kim, S. R. Konda, W. Yu, W. Li, and R. A. Ganeev, "Harmonics generation in the laser-induced plasmas of metal and semiconductor carbide nanoparticles," *Nanomater.* **12**(23), 4228 (2022).
61. R. A. Ganeev, M. Suzuki, M. Baba, M. Ichihara, and H. Kuroda, "Low- and high-order nonlinear optical properties of Au, Pt, Pd, and Ru nanoparticles," *J. Appl. Phys.* **103**(6), 063102 (2008).
62. E. Takahashi, P. Lan, O. D. Mucke, Y. Nabekawa, and K. Midorikawa, "Attosecond nonlinear optics using gigawatt-scale isolated attosecond pulses," *Nat. Commun.* **4**(1), 2691 (2013).
63. A. Kramida, Y. Ralchenko, J. Reader, and NIST ASD Team (2022). NIST Atomic Spectra Database (ver. 5.10), [Online]. Available: <https://physics.nist.gov/asd> [2022, November 1]. National Institute of Standards and Technology, Gaithersburg, MD.
64. R. A. Ganeev, M. Suzuki, M. Baba, H. Kuroda, and T. Ozaki, "Strong resonance enhancement of a single harmonic generated in extreme ultraviolet range," *Opt. Lett.* **31**(11), 1699–1701 (2006).
65. G. Duffy and P. Dunne, "The photoabsorption spectrum of an indium laser produced plasma," *J. Phys. B: At. Mol. Opt. Phys.* **34**(6), L173–L178 (2001).